CSIRO PUBLISHING

www.publish.csiro.au/journals/ijwf *International Journal of Wildland Fire*, 2004, **13**, 49–63

Description of a coupled atmosphere–fire model

Terry L. Clark[A,C], *Janice Coen*[A] *and Don Latham*[B]

[A]National Center for Atmospheric Research, PO Box 3000, Boulder, CO 80307, USA.
[B]USDA Forest Service, Fire Sciences Laboratory, Rocky Mountain Research Station, PO Box 8089, Missoula, MT 59802, USA. Email: djl@montana.com
[C]Corresponding author. Present address: University of British Columbia, Department of Earth and Ocean Sciences, 6339 Stores Road, Vancouver, V6T 1Z4, Canada. Telephone: +1 604 822 0278; fax: +1 604 822 6088; email: tclark@eos.ubc.ca

Abstract. This paper describes a coupled fire–atmosphere model that uses a sophisticated high-resolution non-hydrostatic numerical mesoscale model to predict the local winds which are then used as input to the prediction of fire spread. The heat and moisture fluxes from the fire are then fed back to the dynamics, allowing the fire to influence its own mesoscale winds that in turn affect the fire behavior.

This model is viewed as a research model and as such requires a fireline propagation scheme that systematically converges with increasing spatial and temporal resolution. To achieve this, a local contour advection scheme was developed to track the fireline using four tracer particles per fuel cell, which define the area of burning fuel. Using the dynamically predicted winds along with the terrain slope and fuel characteristics, algorithms from the BEHAVE system are used to predict the spread rates. A mass loss rate calculation, based on results of the BURNUP fuel burnout model, is used to treat heat exchange between the fire and atmosphere.

Tests were conducted with the uncoupled model to test the fire-spread algorithm under specified wind conditions for both spot and line fires. Using tall grass and chaparral, line fires were simulated employing the full fire–atmosphere coupling. Results from two of these experiments show the effects of fire propagation over a small hill. As with previous coupled experiments, the present results show a number of features common to real fires. For example, we show how the well-recognized elliptical fireline shape is a direct result of fire–atmosphere interactions that produce the 'heading', 'flanking', and 'backing' regions of a wind-driven fire with their expected behavior. And, we see how perturbations upon this shape sometimes amplify to become fire whirls along the flanks, which are transported to the head of the fire where they may interact to produce erratic fire behavior.

Introduction

This paper describes the technical design and results of some computational experiments using a coupled atmosphere–fire model. The design features discussed include: fire perimeter tracking; spatial distribution of the fuel; fire propagation treatment; and heat and moisture exchange between the fire and atmosphere.

The two main approaches to modeling fire area perimeter are the continuous plane and point methods. In the continuous plane approach the fire perimeter is represented as a set of expanding curves which are usually taken as ellipses. This approach is based on Huygens' Principle first proposed by Anderson *et al*. (1982) and further developed by Richards (1995) and Richards and Bryce (1995). It is this approach that has been used by Finney (1998) in FARSITE. One of the reasons for the Huygens approach was to get away from point methods in which the fuel bed is represented as a set of cells arranged on a regular grid (e.g. Ball and Geurtin 1992; Vasconcelos and Geurtin 1992). Such point methods generate unrealistic fire shapes because cell-to-cell probabilistic propagation results in shapes that echo the shape of the initial grid pixels (called ghosting) That is, the cells propagate rather than the fire. Typically, point methods are less complex to code than the continuous plane approaches (Richards 1994) but the latter have been shown to provide a more numerically stable framework for operational use.

The current model is designed for inclusion in a coupled fire–atmosphere dynamical code and will be used for research computational experiments over a broad range of resolutions as well as for eventual operational use within a coupled fire–atmosphere system. The method chosen to represent the fire perimeter should meet a number of criteria. Truncation or numerical errors should decrease with increasing resolution. The method must mesh with the heat and moisture budgets of the model. Grid coordinate propagation effects should also be avoided. In this regard it should be recognized that most

 10.1071/WF03043 1049-8001/04/010049

fluid dynamical models have truncation errors that depend to a minor extent on the orientation of the flow with respect to the grids. This level of grid effect might be considered a measure of acceptable truncation error. However, as should become clear, the grid orientation is not the type of issue with the present scheme as it has been with previous point methods because of the number of degrees of freedom added to this scheme. The method chosen should also work well using coarse fuel cells for a broad range of conditions from grass fires to crown fires. The fuel cell resolution should depend more on the variability of the fuel rather than on the nature of the fire.

Finally, the method chosen must be easily adapted to a parallel computing environment.

To meet the criteria, we developed a particle in cell (or tracer) method that has as few empirically determined parameters as possible but one that is complex enough to meet the requirements discussed. This was achieved by using four particles per fuel cell creating quadrilaterals that are used to define a local fire front as well as the area ignited within any fuel cell. As a result, the code is more complex than the continuous plane approaches but satisfies the demanding requirements of the overall modeling system. Numerical artifacts are less than for the Huygens' Principle approaches but computational cost of the tracer approach is higher. However, the increased computational cost is quite small compared to the cost of the fluid dynamic calculations. This fire perimeter approach is neither a continuous nor a point method but a particle in cell approach utilizing local contour advection. It is suited for coupled fire–atmosphere calculations and should not be used for uncoupled operational use. The ability to parallelize the code was achieved by limiting information exchange between fuel cells to immediate neighbors allowing easy application of Message Passing Interface.

To demonstrate the utility of the fire model code, a number of tests were performed using prescribed wind fields with fire–atmosphere coupling turned off. These uncoupled tests include a spot fire expanding in zero ambient wind with homogeneous fuel conditions (perfectly expanding circle), as well as spot fires expanding in fixed winds from a range of directions and grid orientations. Spot fire tests are too simple to provide a robust test of the code so further tests were designed to test the code for failure. These are purely mathematical cases of windmill and alternating wind direction fires. The windmill fire uses a solid rotation wind and is initialized as two broken firelines at right angles. The breaks in the firelines at the center require the code to treat converging firelines. This configuration is certainly unrealistic for natural fires but it supplies a particularly challenging framework for testing the tracer code, providing a range of horizontal wind shears as well as colliding fire fronts. The final uncoupled test was a single line fire with the wind blowing normal to the line but with the wind direction varying sinusoidally along the line changing directions every 6–12 fuel cells. Except for the last test, symmetry conditions were used to locate indexing and conceptual errors in the code.

The final test of the code is its numerical stability when the coupling between the fire and atmosphere is turned on. Experiments presented here include grass and chaparral fires with heavy fuel loads (specific fuel characteristics are given below in the section *Coupled fire–atmosphere experiments*). The range of variability found in the more realistic experiments exceeds the conditions one finds even in a robust series of uncoupled tests. As a result many weaknesses were detected and corrected and again tested by iterating the battery of uncoupled experiments.

The paper is organized as follows. First we present a general overview of the fire–atmosphere dynamics and the fire model. Then we describe the fireline propagation algorithm and then the application of the BEHAVE rate of spread and BURNUP mass-loss-rate algorithms to the particle in cell method. The next two sections present uncoupled and coupled experiments using the combined model and finally we present our conclusions.

Description of the coupled fire–atmosphere model

The interactive model is an extension of the atmospheric fluid dynamics model of Clark (1977, 1979), Clark and Farley (1984) and Clark and Hall (1996), connected with approximations to the BURNUP heat release model (Albini and Reinhardt 1995; Albini *et al*. 1995) and the fire spread algorithms as used in the BEHAVE system (Rothermel 1972; Andrews 1986). The fluid dynamics model solves prognostic equations for momentum, thermodynamic energy, water vapor, and cloud and precipitation variables by advancing these fields in time at grid points in nested spatial domains. These domains within domains can be refined in both horizontal and vertical directions so that, while outer domains resolve atmospheric scales of motion such as fronts and mesoscale convective systems, the inner domains resolve fine scale features such as individual convective clouds and vortices a few meters wide within firelines.

The innermost fluid dynamics model domain is the one that directly interacts with the fire model. The models are fully coupled in that evolving modeled atmospheric information is used to drive the propagation of the fireline, and the heat and moisture from the fire model is released into the modeled atmosphere, greatly changing the atmospheric motions. More precisely, at each time step of the inner model domain, atmospheric wind velocities from the lowest vertical levels of the fluid dynamics model are passed into the fire model where they are used to advance the fireline to a new position. During this time step, fuel is burned both in the fine fuels that carry the flaming front and in slower burning larger fuels behind the front. Heat and moisture from this combustion enter into the fluid dynamics model as heat and moisture fluxes near the surface.

Rectangular fuel cells can be made smaller than the dynamic grid cell by any integer ratio, providing an accurate representation of the spatial variability of the fuel. The increased resolution of the fuel also improves the accuracy (reduces truncation error) of the linear temporal trend assumption used in the mass loss rate treatment as described in subsection *Mass loss rate*.

General structure of the fire code

The fire calculations are performed subsequent to the atmospheric wind update but prior to the thermodynamic advection routines. At the start of each simulation the fire variables such as fuel load, moisture content, and others used in the fire spread and mass loss formulations are specified, as well as the extinction depth over which the fire's sensible and latent heats are distributed in the atmosphere. Using the winds from the atmospheric model, a local contour advection routine is used to update the position of existing firelines. Details of the contour advection routine that uses four particles (or tracers) per fuel cell will be described in later sections.

After the fireline has been updated, the estimated area burning within each fuel cell is used to calculate the mass fraction of dead and down fuel of all sizes in each cell that has burned during the last time step. This procedure uses elements of the BURNUP algorithm (Albini *et al*. 1995; Albini and Reinhardt 1995) and takes into account a specified representative time scale for the fuel in the cell to completely burn. Using the combustion coefficient, the fuel burned in the last time step is converted to latent and sensible heat fluxes.

Although we have not done canopy experiments in this paper, we have built in code for such experiments. Prior to possible canopy ignition, the heat flux from surface fire is entirely absorbed by the canopy. When the canopy is dry, it is ignited at a threshold of $0.17\,\mathrm{MW\,m^{-2}}$. Currently, a canopy fire in the model is collocated with the ground fire, and cannot propagate separately as sometimes occurs in nature when a crown fire races ahead through the treetops. The dry canopy mass corresponding to the change in fractional area of the ground fire is burned and converted to latent and sensible heat. The sensible and latent heats from the ground and canopy for each fuel cell are summed back onto the larger fluid dynamics grid and used as surface fluxes in the atmospheric model.

Fireline propagation

We will now describe details of the fireline advection scheme and how we use the four particles (or tracers) in each fuel cell to track the fireline.

Definition of sub-grid-scale quadrilaterals

Figure 1 shows a basic quadrilateral structure within a fuel cell with tracer particles and equivalent fuel cell corners numbered 1 through 4. The tracers move in a manner defining

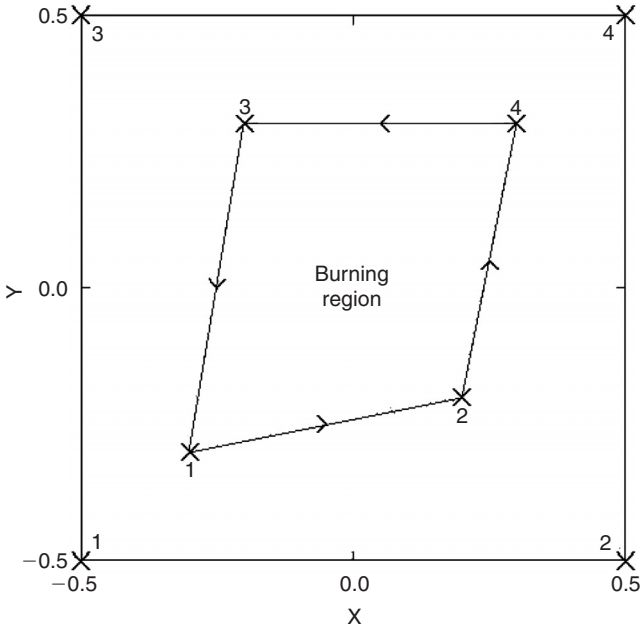

Fig. 1. Basic quadrilateral definition.

a time-dependent burning region within each fuel cell. The tracer motion allows firelines to progress smoothly through the rectangular fuel cells without significant distortion effects due to the finite size and shape of the grid, eliminating ghosting effects. As shown in Fig. 1, the grid is scaled between ± 0.5 in both the x- and y- directions. All four tracers must remain within the boundary of their respective fuel cell, but temporary advection of a tracer outside the boundaries of its fuel cell can occur. For example, it may first pass through the $x = -0.5$ boundary but with $-0.5 > y > +0.5$. This may result in the ignition of the neighboring grid if it is not already burning, followed by the tracer-1 x-coordinate being fixed at $x = -0.5$. Remaining motion of that particular tracer is then confined to the y-direction. The logic is formulated so that all tracers move towards the grid corner with the corresponding number.

Arrows marked in Fig. 1 on lines joining the four tracers define the directional sense of the fireline. As we move along the coordinate positions defining the fireline, the fire will always be on our left with increasing index number. For the illustrated rather special case of a sub-grid-scale spot fire, the tracer positions correspond to the coordinate positions of the fireline. However, due to the sense of progressing along the fireline the fireline numbering would progress 1–2–3–4 at, say, the corresponding tracer points 1–2–4–3, i.e. there is a difference between the tracer position numbering and the sense of fireline progression for the sub-grid-scale case. Normally fires are not treated as sub-grid-scale.

Figure 2 shows the inter-grid definition of the fireline, again with arrows marking the sense of progression with the fire always on the left. In Fig. 2 the central grid

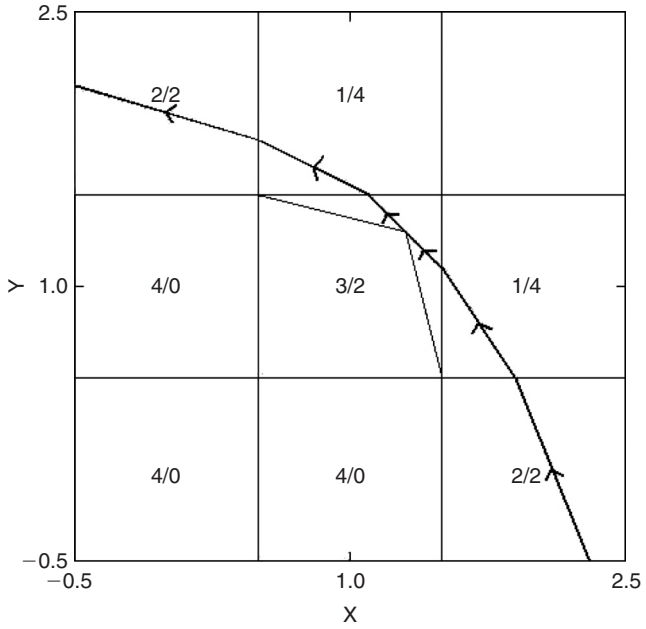

Fig. 2. Fireline definition using neighboring coordinates. Note the use of virtual coordinates to define the fireline for the center fuel cell.

uses coordinates of two neighboring grids to define the fireline within the fuel cell. This is required because the only remaining 'free' tracer is tracer-4 because the other three tracers have reached their limiting corner positions. It takes five tracers to completely define the passage of an arbitrarily oriented linear fireline passing through a fuel cell. If we use virtual points, as in the case shown, we can achieve the same consistent treatment using only four tracers per fuel cell. The use of five tracers per fuel cell would severely complicate the logic.

Also shown in Fig. 2 is the definition of the class of each fuel cell. We use two numbers to define the class (NCT/ICLS). The first number (NCT) refers to the number of tracers at their limiting corner positions. The second number (ICLS) refers to the number of remaining free coordinates. For example, the central grid is referred to as a **3/2**. In this case, three of the four tracers are at their limiting corner positions whereas both the x- and y- coordinates of tracer-4 are still free to move. The neighbor on the right is a **1/4** because tracer-1 is at its corner position, tracer-2 has only a free x-coordinate, tracer-3 a free y-coordinate and tracer-4 has two free coordinates making a total of 4 free coordinates.

The **0/8** class shown in Fig. 1 is not presently active in the code, obviating sub-grid fires. The six classes treated are the **4/0**, **3/1**, **3/2**, **2/2**, **2/3** and the **1/4**. This set is small but complete, providing the fuel grid size is commensurate with the width of the fireline.

Since we use virtual coordinates within cells to define the actual region of fuel ignition we require two definitions of area. The simplest area to define is the area of the quadrilateral, A_q, where

$$A_q = 0.5|\vec{d}_1 \times \vec{d}_2|, \tag{1}$$

where $\vec{d}_1$ and $\vec{d}_2$ are the diagonal vectors. Using coordinate positions,

$$A_q = 0.5[(x_4 - x_1)(y_3 - y_2) + (y_4 - y_1)(x_2 - x_3)]. \tag{2}$$

However, if we consider the central cell in Fig. 2, we must add two minor triangular areas to obtain the full ignition area, A_f. In this case

$$A_f = A_q + 0.5[(x_3 - x_4)(y_4 - y^*) - (y_3 - y_4)(x_4 - x^*)] + 0.5[(x_4 - x_2)(y_4 - y^{**}) - (y_4 - y_2)(x_4 - x^{**})], \tag{3}$$

where the superscripts refer to the appropriate neighbor grid coordinates. Virtual coordinates are used for classes **2/3**, **3/1**, **3/2** but not for classes **4/0**, **2/2**, or **1/4**. The use of virtual coordinates is important for defining the location of the fireline as well as determining the rate of change of area burned when treating the sensible and latent heat exchange between the fire and atmosphere.

Defining the fireline and normal vectors

The first task is to identify all fuel cells that determine firelines. A fuel cell is defined as part of a fireline if it has been ignited and if $A_q < 1 - \varepsilon$, where ε is a small number. However, we do allow cases with $A_q = 1$ provided one or more of the neighboring grids has not been ignited. This case is infrequent but occurs when the fireline lies precisely on a grid boundary. Fireline fuel cells are identified with the flag NFL = 1 and the remaining cells with NFL = 0. Fireline coordinates are assigned to all NFL = 1 cells and neighboring grids (also with NFL = 1) on each side of every fireline fuel cell are identified. Once the neighboring cells have been identified we adjust the coordinate end points by assigning an average value to the overlapping points. Analytically this has no effect on the values of the coordinates, but in the numerical code it eliminates any drift resulting from round-off errors.

Using the above information, normal vectors directed away from the fire are calculated. The normal vector is calculated by first fitting a circular arc to three points. In deriving the arc we always use two fireline end points. Coordinates fit to an arc provide a large enough radius of curvature to give a sufficient degree of numerical stability. It should be noted that, once the limiting radius of fit is specified, its physical dimension decreases with increasing resolution, thus providing the model with consistent truncation error characteristics.

The number of fireline points varies from 2 to 4 depending upon the class of the cell. For example, a **3/1** or **1/4** will both have three points whereas a **4/0** or **2/2** has only two points. Of course the **0/8** shown in Fig. 1 has 4.

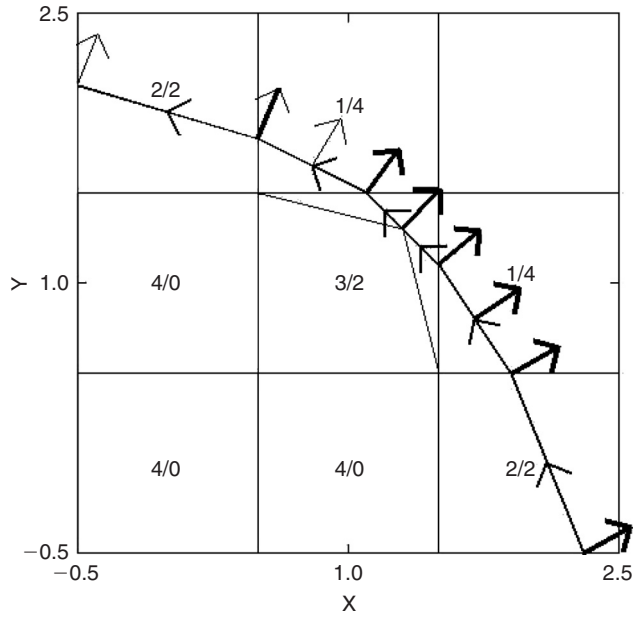

Fig. 3. Same as Fig. 2 except with vectors directed normal to the fireline.

Figure 3 shows the type of calculation resulting from a fireline coordinate identification. This is similar to Fig. 2 except for the addition of the vectors directed normal to the fireline. These normal vectors are used in our fire-spread calculations.

As a validation test on the mathematical formulation, we ran two comparison tests using a spot fire in zero ambient wind. In the first case the normal vectors were calculated analytically using the known circle geometry. The second test used the basic code. Identical results were obtained, indicating that the calculation of the normal vectors was correct.

Fireline spread treatment

A rate of spread is determined at each coordinate point of the fireline. The spread rates depend upon wind speed, terrain slope, atmospheric humidity, fuel type and fuel moisture. In this paper we use the Rothermel formulation (Rothermel 1972). In our previous simulations (Clark *et al.* 1996*a*, 1996*b*) the McArthur formula (Luke and McArthur 1978) was used. The rate of spread algorithm, the mass loss formulation, and heat/moisture flux calculation are described later. Spot fire initiation results in circular shaped burns in zero wind conditions and in cigar-shaped fires with moderate winds.

A future approach to treating the spread rate is to use physically based parameterizations based on model parameters such as temperature gradients, radiation intensity, vortex dynamics and fire winds. Comparison with multi-phase models (Linn 1997) can then be addressed. The present framework should prove particularly useful when considering large fires of long duration where an efficient parameterization approach is required.

Re-establishing fuel cell geometries of ignited cells

After propagating the fireline coordinates to their new positions, we use an algorithm to establish the new coordinates of existing fireline fuel cells. The previous class of each fireline fuel cell is used to define the logic needed to assign new coordinate positions.

The typical procedure is to find points where a fireline segment crosses a fuel cell boundary. Depending on the curvature of the fireline and local wind structure, a neighboring line segment may be used. Points lying solely within a fuel cell may either take their new coordinates directly from the new values or, as in the **1/4** class, the free (or center) coordinate takes an average or mid-point value. For example, the two **1/4** cells shown in Fig. 3 have free tracer-4 coordinates. The tracer-4 positions are taken as the average of the tracer-2 and tracer-3 coordinate positions. This treatment of the free coordinate position of the **1/4** class improves the performance and stability of the scheme. Assignment of the remaining two **1/4** coordinates is achieved by using a combination of neighboring points. A search is made starting with the most stable combination and working through to the least stable until a match is found. By far the least stable scheme is to use only **1/4** coordinates. During the assignment of new quadrilateral coordinates we convert all new cells of class **2/3** to **2/2** class. This conversion is essential to keep all coordinates of a cell meaningful. Again this improves both the performance and stability of the scheme by removing a degree of randomness associated with the free-coordinate position. After reassigning coordinates to existing fuel cells we re-establish the class of all fuel cells.

Ignition of new fuel cells

The process of fuel cell ignition is probably the most difficult and sensitive aspect of the code. Illogical ignition of cells can result in almost immediate failure of the code in the next time step. For this reason a detailed description of the logic of ignition follows.

Identification of new ignitions

We cycle through all fireline cells with NFL = 1 and ask whether any of their new fireline end coordinates moved into neighboring cells. If yes, then we ask whether that cell represents a new ignition.

If a cell is already ignited and there was an attempted re-ignition, then we check for converging firelines. For example, if an ignition occurs across the $x = -0.5$ boundary of a cell with NFL = 1 and corners 1 and 3 of that cell are both unoccupied, then we treat this as convergence of a fireline from the west since part of the eastern boundary of the cell is already burning whereas none of its western boundary is

burning. All converging fireline cells are identified before treatment. A subsequent loop identifies those cells straddled by neighboring cells also slated for ignition due to converging firelines. After these are ignited the remaining cells are treated.

If a particular fuel cell is identified as a fresh ignition we then evaluate which particular fireline segment to use for ignition. A line segment can be ill-defined if it represents the extreme end of a sharply turning region of a fireline. If, for example, a fireline has propagated a very small distance into a cell and its linear extrapolation defines a large fraction of that cell, then ignition is either premature or a neighboring cell may provide a more logical ignition.

The logic used for evaluation is to accept ignitions if extrapolation of the line segment in question encompasses only one corner of the cell being ignited. If it encompasses more than one corner but the area of the igniter cell is larger than 0.95, then we also accept the ignition. The rationale is that this case is almost certainly an ignition by a fireline segment oriented nearly parallel to a coordinate direction.

Choosing cell and coordinate to act as igniter

After determining all acceptable ignitions we must decide on a single ignition for each cell. If a cell has multiple igniters then we simply chose the neighbor cell with the largest burning area as the igniter. The assumption here is that the geometry is more stable in such cases. This logic helps control problematic ignitions by class **1/4** cells.

After choosing cells and their line segments to act as igniters we then determine which fuel cell corners of the ignited cells will be occupied, simply by linearly extrapolating the igniting fireline segment through the fuel cell and identifying which corners lie within the new fireline.

We then use different logic for finalizing the new quadrilateral coordinates depending upon whether one corner or two corners have been ignited. We do not allow for no corners or more than two corners. This limitation affects the maximum time step we can use.

Unresolved islands of fuel

The final procedure in the new ignitions process is to look for poorly resolved islands of fuel. Since the code allows only one fireline per fuel cell the minimum resolvable fuel island is 2 fuel cells in any direction. When an island's dimensions decreases to 2×2 then all four cells are ignited.

Rate of spread and mass-loss rate implementation

The Rothermel algorithm provides a fire spread rate in the form

$$S_f = (1 + \varphi_w + \varphi_s) R_0, \tag{4}$$

where R_0 is the spread rate for zero wind, no slope conditions, φ_w is an adjustment for wind, and φ_S an adjustment for terrain slope. Note that the wind effect is a correction to the rate of spread. The wind used in the Rothermel model is the midflame wind, *that would be there if there were no fire present.* Also, winds in the BEHAVE system are input at the Weather Service Standard height of 20 ft. The BEHAVE system has an internal conversion, assuming a logarithmic boundary layer, to correct the wind value to that used in the Rothermel model. For the interactive code we take the wind at a specified distance above ground level and behind the fireline, correcting to midflame wind. This circumvents the problem that the horizontal atmospheric wind near the surface at the fireline is approximately zero, since this is a line of convergence. In the cases presented, the specified distances were chosen as 5 m behind the fireline and 5 m above the ground. Again, the Rothermel model is used to obtain rate of spread only; energy release is obtained from our approximation to BURNUP. The *e*-folding depth of extinction for the ground heat flux in the atmospheric model (i.e. the depth at which the heat flux has decreased by a factor of *e*) was 50 m.

Table 1. Fuel characteristics used in the experiments

	Tall grass	Chaparral
Dry fuel load	$0.674\,\mathrm{kg\,m^{-2}}$	$3.584\,\mathrm{kg\,m^{-2}}$
Moisture content	7.0%	20.0%
Fuel depth	0.762 m	2.0 m
Surface area to volume ratio (SAVR)	$4921\,\mathrm{m^{-1}}$	(not used)
Oven dry fuel density	$512.6\,\mathrm{kg\,m^{-3}}$	(not used)
Fuel particle effective mineral content (SE)	0.010	(not used)
Fuel particle total mineral content (ST)	0.0555	(not used)
Weighting parameter for mass consumption (BURNUP)	7	180

Chaparral is a fairly unusual fuel in many respects. Based upon our observation that the spread rate in chaparral is overwhelmingly dictated by the environmental wind speed, far more than other fuel factors, for fire spread rate in chaparral we used the simplified approximation:

$$S_f = 1.294\, U^{1.41}, \tag{5}$$

which is capped at a maximum spread rate of $6\,\mathrm{m\,s^{-1}}$. When the component of wind normal to the fireline is zero, the backing rate of spread for chaparral is specified as $0.0333\,\mathrm{m\,s^{-1}}$. For other fuels, the backing rate is calculated using the Rothermel spread rate for no wind on flat ground.

Fuel parameters

Two types of fuel were used in these experiments, tall grass and chaparral. Fuel characteristics distinguishing each are shown in Table 1. The fuel types used here are not formal BEHAVE fuel models, but do have some parameters in common. As stated earlier, we use the approximation, equation (5), to calculate the spread rate only for the fuel type chaparral. This formula depends only on environmental

wind speed; thus, some fuel characteristics in the last column of Table 1 need not be specified.

Mass loss rate

The rate at which fuel is consumed, once it is ignited, is described using a mass loss parameterization. The parameterized spread rate is used to determine the ignited area and a BURNUP-type curve (Albini 1994) provides the fraction of fuel remaining as a function of time after time of ignition.

The propagation of the fireline through a fuel cell means that points within the cell will have been burning for different lengths of time. To determine the fractional mass loss f_b over a time step, we estimate the time history of the area burned in the fuel cell and integrate to calculate the currently remaining fuel mass.

The equations describing fuel mass and mass loss are

$$m(t) = m_0\ f_b\ (t) \tag{6}$$

or

$$\frac{\partial m}{\partial t} = m_0\ g_b\ (t), \tag{7}$$

where $g_b(t) = \partial f_b/\partial t$. Since $f_b(t)$ is an asymptotically decreasing function with increasing time, its time derivatives are reasonably smooth allowing accurate fits using combinations of low order polynomials, exponentials or Pade approximates.

Since we have to ascribe a fractional mass loss to each fuel cell of the model whose area is changing with time we cannot use equation (7) directly. Instead we must estimate the time history of the area burned in the fuel cell and from that calculate the remaining fuel mass. Using equation (7), we obtain the double integral

$$F(t) = m_0 \int_0^t \frac{dA(\tau)}{d\tau} \int_0^{t-\tau} g_b(\psi) d\psi\, d\tau \quad \text{for } t \le t_c, \tag{8}$$

where $A(\tau)$ is the ignited area of the fuel cell at $t = \tau$, m_0 is the initial fuel mass and $F(t)$, where $F(t) = 1 - m(t)$, is the mass of fuel burned at time t. Equation (8) is valid only for $t \le t_c$, where t_c is the time at which all the fuel in the cell is burning, i.e. $A(t_c) = 1$. For $t > t_c$ we apply

$$F(t) = F(t_c) + m_0 \int_{t_c}^{t} \int_{t_c}^{t-\tau} g_b(\psi) d\psi\, d\tau \quad \text{for } t \ge t_c. \tag{9}$$

As an example we let the mass loss rate function, $g_b(t)$, be approximated as an exponential where

$$g_b(t) = \frac{1}{W} \quad \exp(-t/W), \tag{10}$$

where W is a weighting factor specified for each fuel type. W is selected such that it approximates the rate of mass loss that would be calculated by the BURNUP algorithm (Albini and Reinhardt 1995). The constraint

$$\int_0^\infty g_b(\tau) d\tau = 1 \tag{11}$$

must be satisfied.

Using equation (10) in equations (8) and (9), we obtain

$$F(t) = m_0 A(t)[1 + \frac{W}{t}\ (\exp(-t/W) - 1] \quad \text{for } t \le t_c \tag{12}$$

and

$$F(t) = m_0[1 + W/t_c\ \exp(-(t - t_c)/W) \times (\exp(-t_c/W) - 1)] \quad \text{for } t \ge t_c. \tag{13}$$

To apply equations (8) and (9) we need to make t_c a field variable. In this manner we can estimate smoothly varying functions of $F(x, y, t)$.

The mass remaining as a function of time is assumed to decrease exponentially, an approximation to the general curve produced by the BURNUP algorithm. Figure 4 shows curves of $f_b(t)$ *v. t* for the two fuel types of tall grass (fuel type-3, $W = 7$) and chaparral (fuel type-4, $W = 180$).

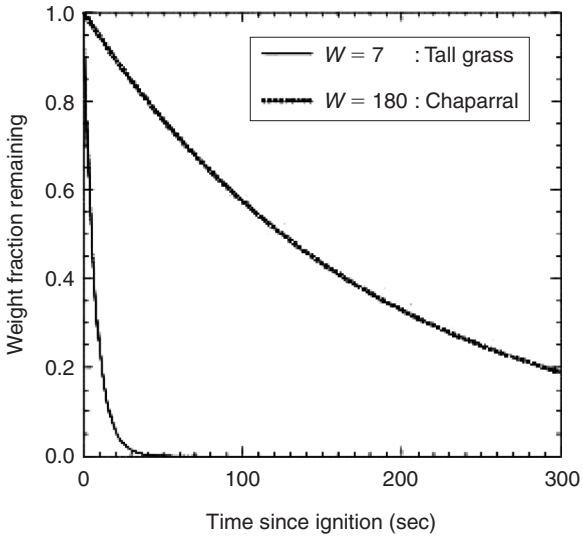

Fig. 4. Mass-loss curve for tall grass ($W = 7$) and chaparral ($W = 180$). Curves show the fraction of initial fuel remaining after time of ignition.

Uncoupled tests of the fire model using specified winds

We define 'uncoupled tests', as simple tests using specified, fixed winds to spread the fire instead of allowing fire–atmosphere coupling. Feedback of sensible and latent heat fluxes into the atmospheric dynamics, which would in turn affect the fire's spread, is not considered.

We employ three types of uncoupled tests to assess the performance of the fire model. The first is the spot fire in

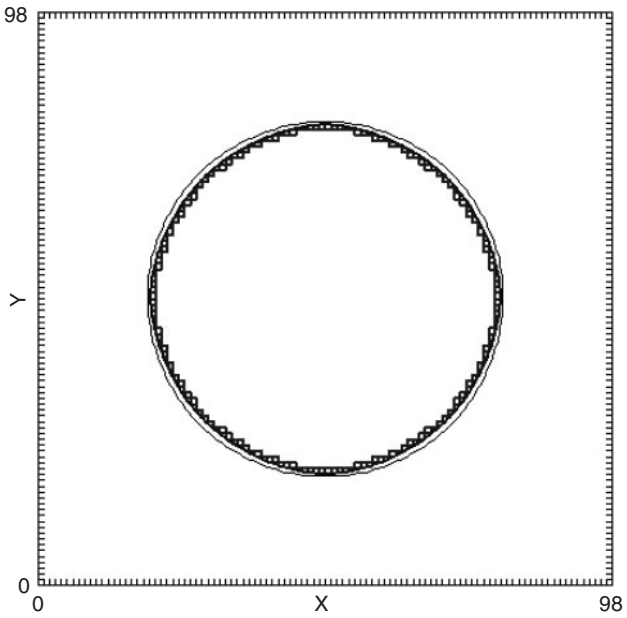

Fig. 5. Fire spread in zero ambient wind. Fire boundary fuel cells are shown and logical fire boundary is shown as a thick solid line. The thin solid line shows the analytical solution.

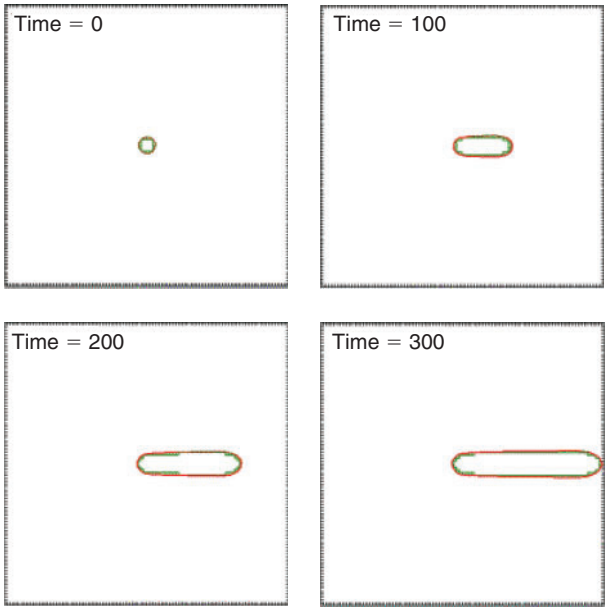

Fig. 6. Same as Fig. 5 except with a $3\,\mathrm{m\,s^{-1}}$ west wind (North is toward the top of the figure).

either zero or constant ambient wind conditions. The second is a so-called windmill fire where the initial conditions are taken as four line segments forming an open cross. The wind for this case is taken as solid rotation about the center of the cross. The third type uses a spatially oscillating wind. These three uncoupled types of tests provide a robust test on the overall code performance.

Spot fire test

Figure 5 shows the evolution of a spot fire in zero wind conditions. The figure shows the model forming a circle with only minor artifacts resulting from grid effects. The solution is symmetric with all quadrants giving identical solutions, which is a necessary condition for the code. A minor but systematic directional difference between the analytical and numerical solutions can be seen by comparing the thin and thick solid lines.

Figure 6 shows a similar sequence to Fig. 5 of a spot fire evolving in ambient westerly wind conditions. As a result of the Rothermel formula the fire spreads much faster in the direction of the wind compared to against the wind, resulting in cigar shaped fires. Figure 7 shows results for a south-west and southerly flow for the same case at $t = 200$ s, again using a $3\,\mathrm{m\,s^{-1}}$ wind speed. Comparison of Fig. 6 and Fig. 7 show that the solutions rotate with the wind to an accuracy of truncation error level showing no significant differences between these cases.

The spot fire tests provide quite limited tests of the fire code. For example, the fact that all the spot fire simulations shown have diverging fireline coordinates means that significant portions of the code are not active. The next two uncoupled tests (line fire and windmill case) provide more robust tests because of the local variations in wind speed and direction and the presence of both converging and diverging firelines.

Line ignition in an oscillatory wind field

In this case the fire is ignited along a straight north–south line in the presence of strongly varying wind. The wind varies in a sinusoidal pattern between westerly and easterly flow (speed shear) using a wavelength of 12 fuel grids. The maximum wind speed was taken as $3\,\mathrm{m\,s^{-1}}$. This test revealed a number of weaknesses of the code, particularly in the treatment of the 1/4 class.

Figure 8 shows four times between $t = 10$ and 400 s. Evident in the figure are the development of long protrusions resulting from the variations between wind driven and backing conditions. Although no systematic testing has been performed, this test offers the utility to assess the inherent diffusion levels of the tracer scheme.

Windmill test

Another idealized but extremely challenging uncoupled test was devised using a cross-shaped fire in solid rotation flow. We call this the 'windmill' test because the fire takes on the shape of a four-bladed windmill. The fires are initiated at a finite radius from the domain center resulting in four separate firelines converging towards each other at the center. This convergence at the center eventually results in an isolated fireline burning inwards towards the center and tests the code on a fireline having the opposite sense of curvature

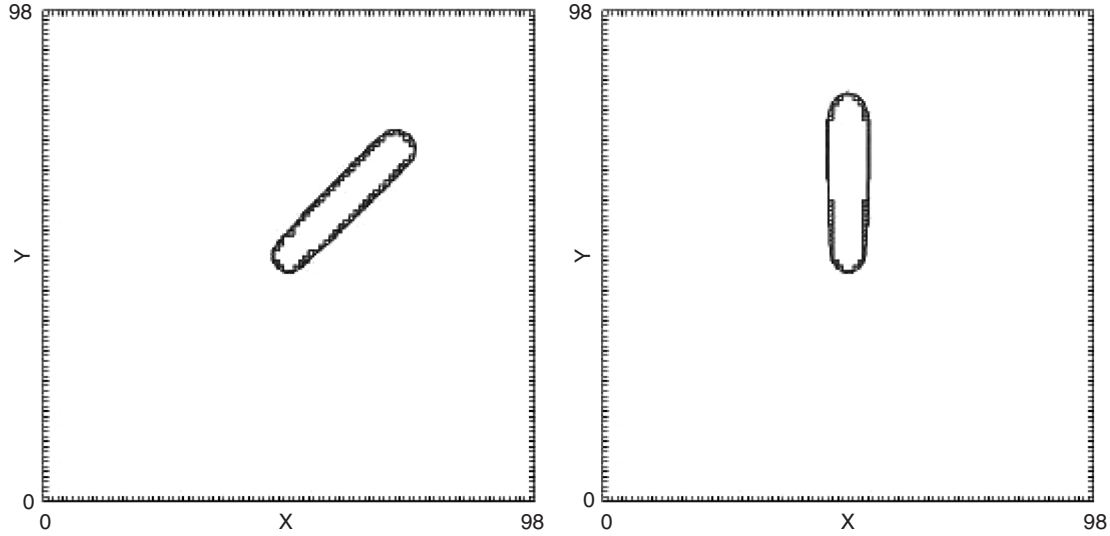

Fig. 7. Two cases showing model results for winds from the south-west and south.

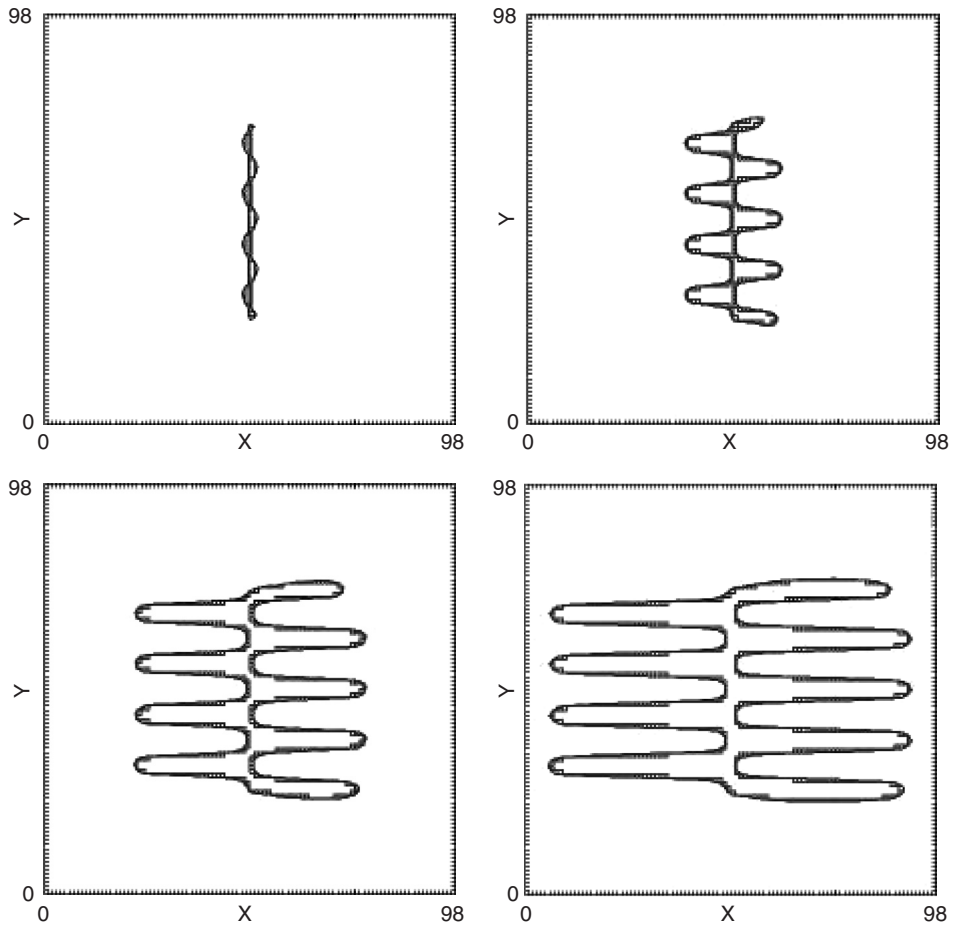

Fig. 8. Four time sequences from the line fire in the oscillatory wind field. Times shown are 10, 100, 250 and 400 s.

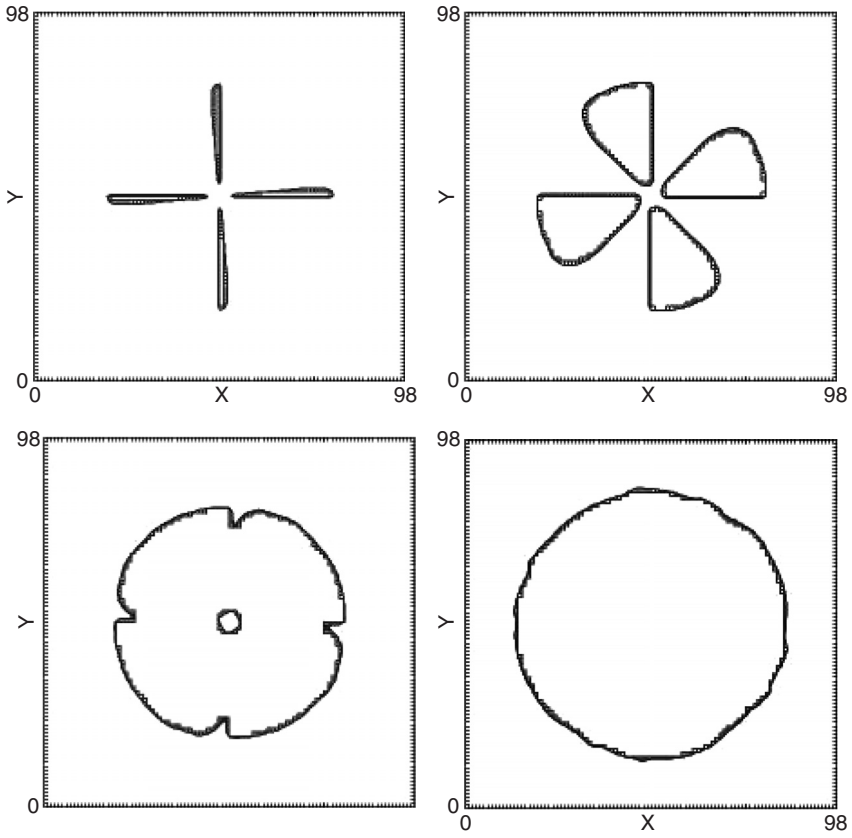

Fig. 9. Windmill test results at $t = 10$, 100, 200, and 560 s, respectively. Active fireline quadrilaterals are shown and a solid line outlining the fireline is also shown.

than is typical. Again, symmetry tests are used between the four different 'blades' of the windmill to assess the logical consistency of the code.

Figure 9 shows four sequences from the windmill fire. The plot at $t = 10$ s shows the initial conditions with four linear firelines making the shape of a cross but with separation at the center. At $t = 100$, the fires have taken on a windmill shape with the fires propagating farther in the faster ambient flow. By $t = 200$ all the firelines have converged leaving a small circular shape in the center of the domain. By $t = 560$ almost all the fuel has been burned within the center of the domain and the four separate fires have merged into a circular shape. Figure 10 takes a closer look at how the model treats fire spread for converging firelines.

Figure 10 shows a time sequence near the center of the domain emphasizing the code treatment of the four converging firelines. Figure 10 also shows the evolution of the fireline at junctions formed by the back burn and forward burn of neighboring windmill blades.

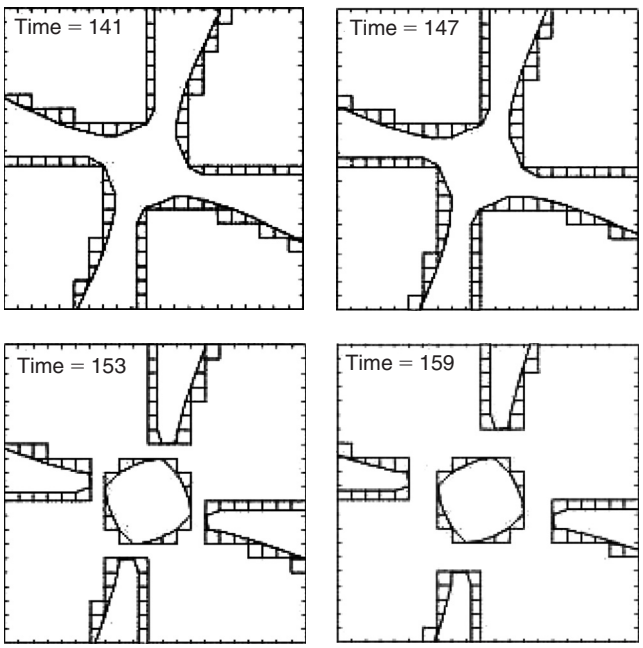

Fig. 10. Results of windmill test near center of domain. Times shown are $t = 141$, 147, 153 and 159 s emphasizing the convergence of four firelines.

Coupled fire–atmosphere experiments

Having tested the adaptations of the Rothermel algorithm and BURNUP, as well as the stability of the tracer sub-grid

Table 2. Description of the model geometries

(*a*) The mountain half-width was taken as 300 m for a Gaussian shaped ridge. The maximum slope is 0.858 $h_0/a = 57.2\%$ or 30° for the cases with $h_0 = 200$ m. H_{bl} is the height of the boundary layer. Δx_d and Δx_f are the horizontal grid sizes used (both *x*- and *y*-directions) for the dynamic model and the fuel cells or fire model. NMDLS is the number of domains. NLVL is the number of absorber levels for the outermost domain

(*b*) *N* is the domain number. *NX*, *NY* and *NZ* are the number of grid points in the *x*-, *y*- and *z*-directions. *H* is the height of the outer most domain. Δx, Δy, and Δz are the grid increments in the *x*- *y*- and *z*-directions, respectively

(*a*)	Expt type	NMDLS	h_0 (m)	H_{bl} (km)	$\Delta x_d/\Delta x_f$ (m)	$\Delta z_{\min}$ (m)	NLVL
	Flat	3	200.0	2	20/10	10	11
	Small hill	3	0.0	2	20/10	10	11

(*b*)	*N*	*NX*	*NY*	*NZ*	Δx (m)	Δy (m)	Δz range (m)	*H* (km)
	1	72	72	58	120	120	13–250	7.88
	2	86	86	78	40	40	7–70	4.08
	3	142	142	64	20	20	4–28	1.03

parameterization, we turned to experiments using the coupled models. Although a set of simple experiments on the flat, on an incline, and the like, would have been preferable, the exigencies of available funds and computer time on the mainframe necessary to carry out the fully coupled model prevented these. We chose to do fire on the flat and on a Gaussian shaped ridge to see if the coupled system gave results that demonstrate observed behavior of actual fires.

Description of experiments

Table 2 describes the various experiments using the coupled fire–atmosphere code. These idealized experiments examine a fireline propagating up the relatively sharp slope of a small hill of Gaussian cross-section shape (height 200 m, half-width 300 m). The hill extends north–south over the entire modeling domain. We initialized a 409 m linear fireline to the west of this hill. The ambient flow had constant 3 m s^{-1} wind from the west (left). The atmospheric temperature structure was stable with a potential temperature lapse rate of 10 degrees per km.

Each of the four simulations used three nested domains as shown in Table 2. The domains, from outer to inner, were 8.4 × 8.4 km (with 120 m grid spacing), 3.36 × 3.36 km (with 40 m grid spacing), and 2.8 × 2.8 km (with 20 m grid spacing). There is 2 : 1 vertical grid refinement between each domain. The naming of the four experiments is shown in Table 3. In all four experiments, the heat from the fire is deposited into the atmospheric over a 50 m extinction depth.

Table 3. List of experiments

	Grass	Chaparral
Flat ground	GRFT	CHFT
Hill	GRHL	CHHL

Results: fire on flat terrain

Figure 11 shows results from Experiment CHFT, that of a fire in chaparral on flat terrain. The fire is initialized as a 400 long line (Fig. 11*a*), in uniform 3 m s^{-1} westerly winds (from the left). As the fire evolves (Fig. 11*b*–11*d*), it takes on a shape well-recognized in real fires, that of a bow or ellipse of fire surrounding the ignited and burned fuel. The fireline itself has three regions: (1) the 'head', the fastest moving, leading edge of the fire where the heat is focused; (2) two 'flanks' along the side where the winds blow almost parallel to the fireline; and (3) the 'back', the slowest moving part of the fire that creeps into the wind. The heat produced by the fire rises in updrafts that the winds focus at the head. These updrafts draw warm air into their base from all directions, guiding the wind to flow along the flanks and focus the heat at the front. This creates a self-perpetuating shape—for example, because the winds along the flanks are essentially parallel to the fireline, this region spreads relatively slowly to the head, where winds are directing the fireline into fresh, unburned fuel. Thus, the largest heating rates are at the head, creating the dominant convective updraft that draws air in at the surface from all sides, creating winds that blow along rather than across the flanks. Similarly for the fire back—although the environmental winds generally determine which edge of the fire is the head, the convective updrafts at the head draw air over the back of the fire in such as way as to oppose its spread into unburned fuel, limiting its spread rate and heating, and thus its dynamic impact on fire behavior. As pointed out by Albini (1993) 'It is a remarkable fact that the general shape is the same for a savanna fire, a shrub fire, or a timber

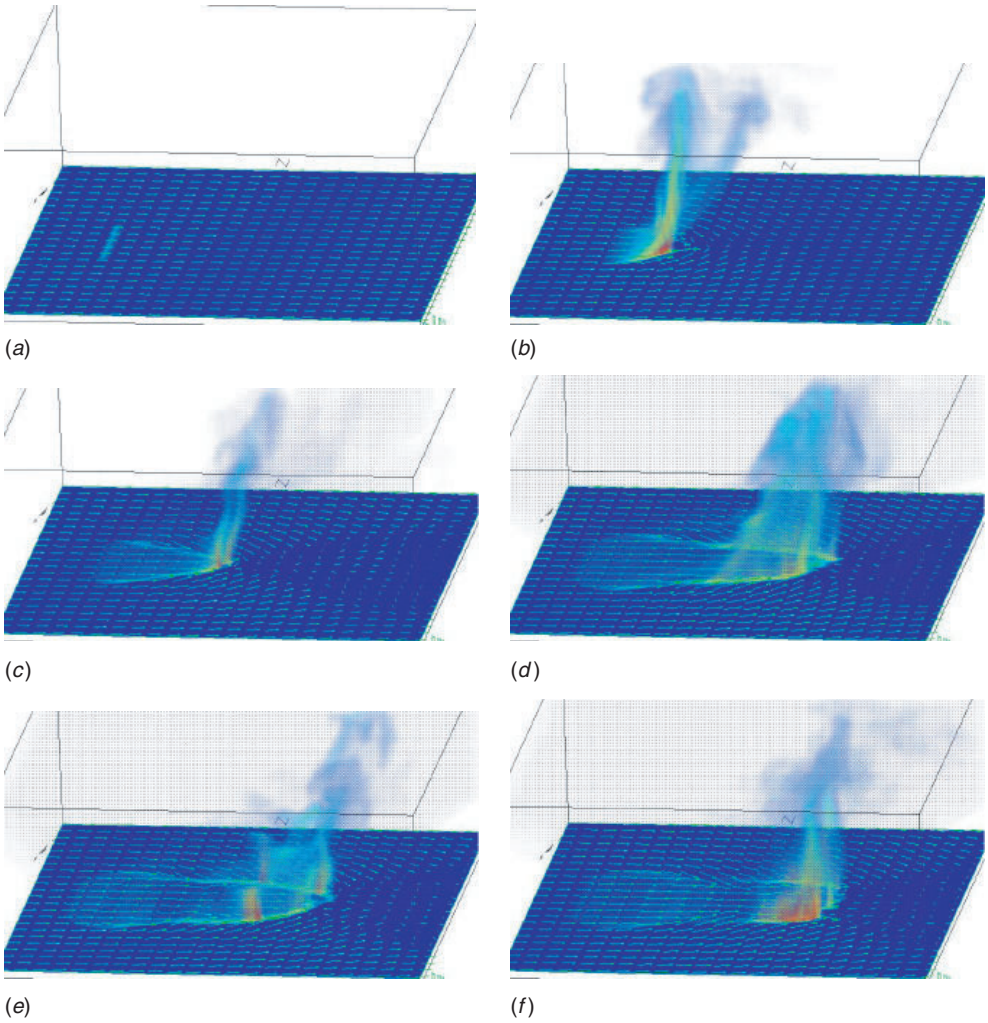

Fig. 11. Plots of three-dimensional buoyancy (volume rendered), two-dimensional shaded contour of buoyancy at 3 m AGL, and horizontal wind vectors at 3 m AGL at six times from initialization. (*a*) 0:06 (6 s); (*b*) 5:24; (*c*) 20:42; (*d*) 1:05:00; (*e*) 1:07:48; (*f*) 1:08:54. The domain's dimensions are 2.8 km × 2.8 km × 1.03 km. Vectors are shown every sixth gridpoint.

crown fire'. Although not all the complexity of a fire has been represented in the model, we can see the fundamental shape characteristics arise in even simple experiments and are a direct consequence of fire–atmosphere interactions.

Although this simulation presents a fireline that maintains this somewhat steady shape for an hour of simulation, perturbations can and do occur. (In nature, this might be due to fuel or terrain inhomogeneities. In computations, very small perturbations might occur at machine error level. In both cases, these might amplify due to the inherently non-linear dynamic processes.) A perturbation in the velocity field along the fireline can produce a local perturbation in the spread rate into unburned fuel, and consequently one in the buoyancy (increasing horizontal vorticity) and updraft (which tilts and stretches the horizontal vorticity), producing a fire whirl. These fire whirls (Fig. 11*e*–11*f*) amplify and propagate downwind along the flanks toward the head, where interaction with others may break up the overall fireline shape.

Results: Fires on hills

The unusual variations in the fire shape can be explained in terms of fire–atmosphere interactions. We first see in Fig. 12 that the fire takes on a well defined parabolic or pointed shape up to about $t = 20$ min while still climbing towards the crest of the hill. The most likely cause of the development of this shape is the convergence zone produced by the convection in front of the fire, causing the heading speed to be much faster than the flanking speed, as described in the simulations of Clark *et al.* (1996*a*, 1996*b*). This convergence effect depends on the rate of heat release in the interior of the fire and on how far ahead of the fire the external winds displace the location of surface convergence. Numerical experiments have shown

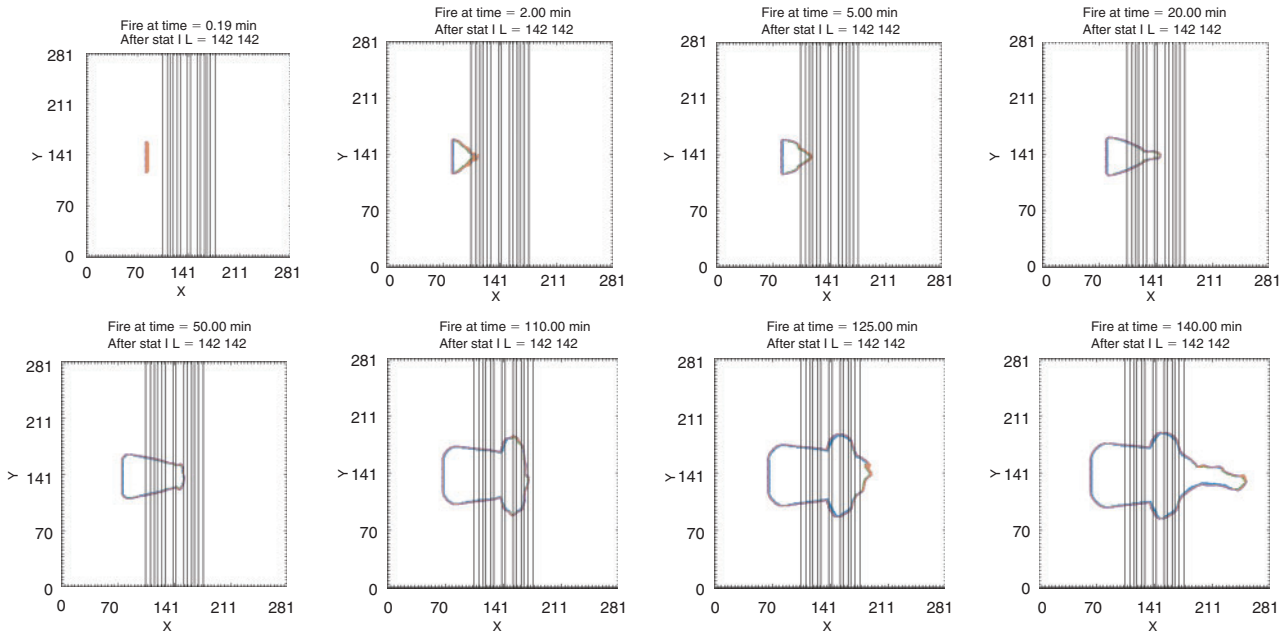

Fig. 12. Fire perimeter for experiment GRHL at the eight times of 0, 2, 5, 20, 50, 110, 125 and 140 min, respectively.

that varying these parameters can cause fires to experience a range of feedback behavior from 'plume' to 'wind-driven'.

From $t = 20$ to about $t = 110$ min we see some effect of the mountain affecting the fire behavior. As the fire approaches the ridge, the fire bulges out along the ridge as a result of the upslope winds on the lee of the slope reducing the heading speed. These enhanced inflow winds result from interactions between the fire winds and the terrain. However the heat released by the grass fire is not sufficient to cause a particularly strong effect in this case so, after $t = 110$ min, the fire continues over the ridge and propagates out over the plains. At $t = 140$ min we see that the fire has lost some of it symmetry as a convective finger moves a little towards the south. It is quite common in fluid dynamics for flows to develop such asymmetries when there is no restoring force to counter any asymmetrical forcing. The forcing in this case could be truncation and/or round-off error. Small artifacts in the fire code might also be responsible. This type of behavior highlights some of the predictive limitations we might expect for fire propagation.

Early development of the chaparral fire is similar to the grass fire in that the fire–convection interaction creates a pointed fire. Figure 13 shows a series of plots similar to those of Fig. 12 but for the chaparral fire where the heat release is considerably stronger than for the grass fire. The plots in Fig. 13 are spaced about 1 min apart to show the rapid development as the fire approaches the ridge-line. The interaction between the fire and terrain is much stronger than for the grass fire because of the significant increase in heat provided by the heavy fuel load of the chaparral. In this case the mountain–fire interaction basically stalls the fire a little to the upwind side of the ridge and allows only a protruding finger of fire to propagate towards the ridge-line. Again the flow is initially diverted to the south with some apparent recovery at later times in the figure.

It appears that the hill acted to funnel the convective updraft toward the center of the fire's head, where the convergence created strong surface winds at the updraft base that increased the spread rate which in turn increased the rate of fuel consumption. This positive feedback effect increased the updraft strength and led to a narrow, rapidly spreading fire head.

Conclusions

One of the classical tests of fire perimeter treatments is to evaluate how well they reproduce known solutions. The fixed wind uncoupled tests demonstrate that the new tracer approach accurately reproduces known fire behavior. Spot fires in zero wind were shown to expand as almost perfect circles and with wind formed the expected elongated cigar shapes. The fire shapes were shown to be quite insensitive to a rotation of the wind. More severe tests were presented such as the highly idealized but computationally demanding windmill fire and the alternating wind direction line fire. The suite of tests presented in this report make a useful framework for comparing alternative schemes in the future. In this new approach, the main effects of fuel cell resolution are better resolution of fuel distribution and more accurate temporal solutions to the double integrals used in the mass loss rate treatment.

Following the BURNUP approach, a rate of mass loss treatment was presented. This is an integral part of the

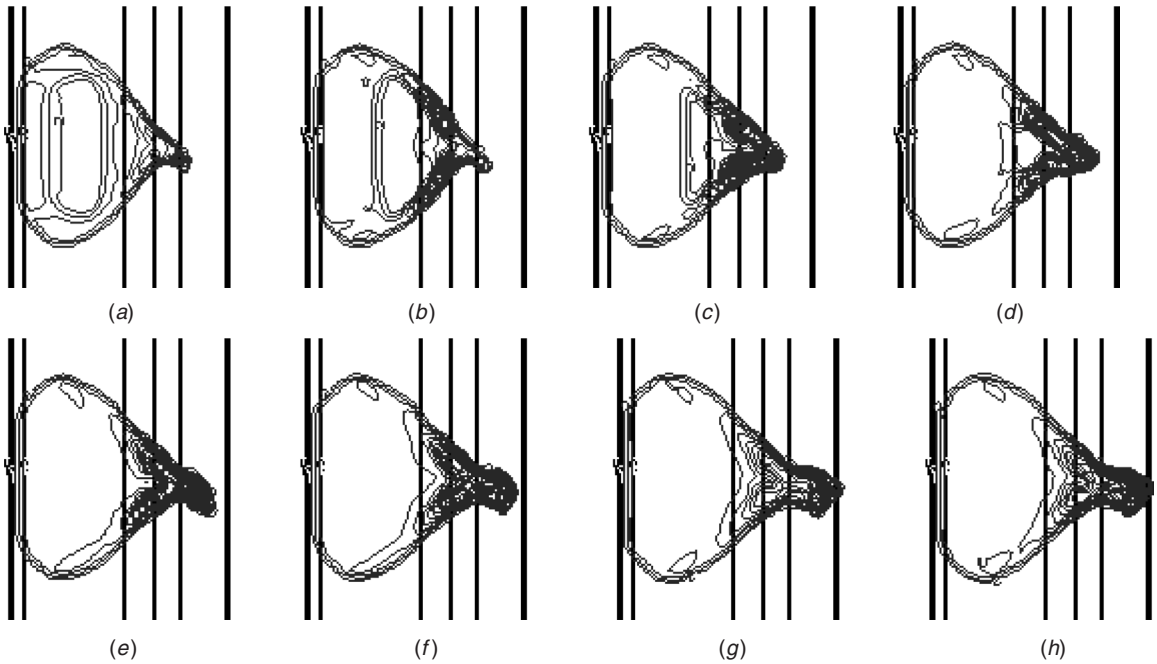

Fig. 13. Buoyancy (contours every 2°) at eight times (61–68 min at 1 min intervals) in experiment CHHL. The fire area is approximately 0.6 km north to south and east to west at this point. The solid lines are topography contours at 50 m intervals; the thickest line at the right of each image is the hill crest.

fire–atmosphere sensible and latent heat exchange treatment. It was shown that this approach, along with the tracer fire perimeter algorithm, allows the model to simulate a broad range of fires from grass fires to chaparral fires without any significant constraints on fuel cell resolution. The width of the fireline remains narrow through the fuel cell parameterized treatment of area burning. The net heat exchange between the fire and atmosphere is largely independent of fuel cell resolution.

The fire perimeter tracer code was applied to a number of coupled fire–atmosphere simulations for both grass and chaparral fires. Typical fire shapes were found to develop for all of our coupled fire–atmosphere experiments that used line ignitions. This is attributed to an interaction between the atmospheric convection and the fireline winds resulting from moderate ambient winds driving the fires (Clark *et al.* 1996*a*, 1996*b*). A noticeable result of this convective interaction between the fire and atmosphere is a pronounced alignment of the flow with the fireline along its flanks. This, of course, results in slow rates of outward expansion along the flanks. During the evolution of these fire shapes we also obtained intermittent convective fingering where narrow fireline protrusions would burst forward and then later rejoin the main fire. The uncoupled tests of the tracer code also resulted in strongly curved leading edges of the fireline for the spot fire ignitions in constant ambient wind. However, this shape is attributed to the simple geometry of the simulations and has nothing to do with interactions between the fire and the atmosphere.

Experiments performed with the coupled fire–atmosphere model also display some important interactions, including showing how the well-recognized elliptical fireline shape is a direct result of fire–atmosphere interactions that produce the ‘heading’, ‘flanking’, and ‘backing’ regions of a wind-driven fire with their expected behavior. Perturbations on this shape would sometimes amplify and lead to fire whirls along the flanks that were transported to the head, where they might interact to break up the fireline. These types of dynamic interactions were particularly interesting in mountainous terrain. Both the grass and chaparral fires stalled when approaching the mountain crest because of the fire induced ventilation winds coming up the opposite side of a ridge-line attempting to block the fire from propagating over the hill. This effect which more pronounced in simulations not shown in this paper that use real topography. Examples are experiments using the terrain of the Dandenong mountains east of Melbourne Australia and the Rocky Mountain Trench in British Columbia, Canada. These simulations will be reported on later. However, even our idealized cases with the 200 m hill demonstrate this effect which is an important consideration to fire managers in mountainous terrain.

Acknowledgements

We thank Francis Fujioka of the Riverside Fire Laboratory, USDA Forest Service, for his partial support of the work carried out in this paper. This work was supported in part by funds provided by the Rocky Mountain Research Station, USDA Forest Service (Research Work Unit RMRS-4401) and the

Riverside Fire Laboratory, USDA Forest Service (Research Work Unit PSW-4401).

References

Albini FA (1993) Dynamics and modeling of vegetation fires: observations. In 'Fire in the environment'. (Eds PJ Crutzen and JG Goldammer) pp. 39–52. (Wiley: New York)

Albini FA (1994) PROGRAM BURNUP: A simulation model of the burning of large woody natural fuels. Final report on Research Grant INT-92754-GR by USFS to Montana State University, Mechanical Engineering Department.

Albini FA, Brown JK, Reinhardt ED, Ottmar RD (1995) Calibration of a large fuel burnout model. *International Journal of Wildland Fire* **5**, 173–192.

Albini FA, Reinhardt ED (1995) Modeling ignition and burning rate of large woody natural fuels. *International Journal of Wildland Fire* **5**, 81–91.

Anderson DH, Catchpole EA, de Mestre NJ, Parkes T (1982) Modelling the spread of grass fires. *Journal of the Australian Mathematical Society B* **23**, 451–466.

Andrews PL (1986) BEHAVE: Fire behavior prediction and fuel modeling system–BURN subsystem Part 1. USDA Forest Service, Intermountain Research Station General Technical Report INT-194. (Ogden, UT) 130 pp.

Ball GL, Geurtin DP (1992) Improved fire growth modeling. *International Journal of Wildland Fire* **2**(2), 47–54.

Clark TL (1977) A small-scale dynamic model using a terrain-following coordinate transformation. *Journal of Computational Physics* **24**, 186–215.

Clark TL (1979) Numerical simulations with a three-dimensional cloud model: lateral boundary condition experiments and multicellular severe storm simulations. *Journal of Atmospheric Sciences* **36**, 2192–2215.

Clark TL, Farley WR (1984) Severe downslope windstorm calculations in two and three spatial dimensions using anelastic interactive grid nesting: a possible mechanism for gustiness. *Journal of Atmospheric Sciences* **41**, 329–350. doi:10.1175/1520-0469(1984)041<0329:SDWCIT>2.0.CO;2

Clark TL, Hall WD (1996) On the design of smooth, conservative vertical grids for interactive grid nesting with stretching. *Journal of Applied Meteorology* **35**, 1040–1046. doi:10.1175/1520-0450(1996)035<1040:TDOSCV>2.0.CO;2

Clark TL, Jenkins MA, Coen J, Packham D (1996*a*) A coupled atmospheric–fire model: convective feedback on fire line dynamics. *Journal of Applied Meteorology* **35**, 875–901. doi:10.1175/1520-0450(1996)035<0875:ACAMCF>2.0.CO;2

Clark TL, Jenkins MA, Coen J, Packham D (1996*b*) A coupled atmospheric–fire model: convective Froude number and dynamic fingering. *International Journal of Wildland Fire* **6**, 177–190.

Finney M (1998) FARSITE: Fire Area Simulator–model development and evaluation. USDA Forest Service, Rocky Mountain Research Station Research Paper RMRS-RP-4. (Fort Collins, CO) 47 pp.

Linn RL (1997) A transport model for prediction of wildfire behavior. Los Alamos National Laboratory thesis LA-13334-T. (New Mexico State University) 195 pp.

Luke RH, McArthur AG (1978) 'Bushfires in Australia.' (Australian Government Publishing Service: Canberra) 359 pp.

Richards GD (1995) A general mathematical framework for modelling two-dimensional wildland fire spread. *International Journal of Wildland Fire* **5**, 63–71.

Richards GD, Bryce RW (1995) A computer algorithm for simulating the spread of wildland fire perimeters for heterogeneous fuel and meteorological conditions. *International Journal of Wildland Fire* **5**, 73–79.

Richards GD (1994) The properties of elliptical wildfire growth for time dependent fuel and meteorological conditions. *Combustion Science and Technology* **95**, 357–383.

Rothermel RC (1972) A mathematical model for predicting fire spread in wildland fuels. USDA Forest Service, Intermountain Research Station Research Paper INT-115. (Ogden, UT) 41 pp.

Vasconcelos MJ, Geurtin GP (1992) FIREMAP–simulation of fire growth with a geographic information system. *International Journal of Wildland Fire* **2**(2), 87–96.